



# CHORUS

This is the accepted manuscript made available via CHORUS. The article has been published as:

## Coupling of Spinons with Defects and Phonons in the Spin Chain Compound $\text{Ca}_{2}\text{CuO}_{3}$

Xi Chen, Jesús Carrete, Sean Sullivan, Ambroise van Roekeghem, Zongyao Li, Xiang Li, Jianshi Zhou, Natalio Mingo, and Li Shi

Phys. Rev. Lett. **122**, 185901 — Published 6 May 2019

DOI: [10.1103/PhysRevLett.122.185901](https://doi.org/10.1103/PhysRevLett.122.185901)

# Coupling of spinons with defects and phonons in spin chain compound $\text{Ca}_2\text{CuO}_3$

Xi Chen,<sup>1</sup> Jesús Carrete,<sup>2</sup> Sean Sullivan,<sup>1</sup> Ambroise van Roeye,<sup>3</sup> Zongyao Li,<sup>1</sup> Xiang Li,<sup>1</sup> Jianshi Zhou,<sup>1,4</sup> Natalio Mingo,<sup>3</sup> and Li Shi<sup>1,4,\*</sup>

<sup>1</sup> Materials Science and Engineering Program, Texas Materials Institute, The University of Texas at Austin, Austin, Texas 78712, USA

<sup>2</sup> Institute of Materials Chemistry, TU Wien, A-1060 Vienna, Austria

<sup>3</sup> LITEN, CEA-Grenoble, 17 rue des Martyrs, 38054 Grenoble Cedex 9, France

<sup>4</sup> Department of Mechanical Engineering, The University of Texas at Austin, Austin, Texas 78712, USA.

\*lishi@mail.utexas.edu

## Abstract:

Extrinsic spinon scattering by defects and phonons instead of intrinsic spinon-spinon coupling is responsible for resistive magnetic heat transport in one-dimensional (1D) quantum magnets. Here we report an investigation of the elusive extrinsic effect in **the** 1D Heisenberg  $S=1/2$  spin chain compound  $\text{Ca}_2\text{CuO}_3$ , where the defect concentration is determined from the measured specific heat and first-principles calculations are used to separate the lattice component of the measured thermal conductivity to isolate a large magnetic contribution ( $\kappa_m$ ). The obtained temperature-dependent spinon-defect and spinon-phonon mean free paths can enable a quantitative understanding of both  $\kappa_m$  and the **spinon-induced Spin Seebeck effect**.

Quasi one-dimensional (1D) magnetic spin systems exhibit a rich variety of physical phenomena, such as superconductivity [1], spin-orbital separation [2], the spin Seebeck effect (SSE) [3, 4], and spin entanglement [5]. Among these 1D systems, the  $S = 1/2$  Heisenberg spin chains with antiferromagnetic coupling between adjacent spins are of particular interest. The elementary spin excitations in these systems are referred as spinons with spin = 1/2. As a result of the integrability of the  $S = 1/2$  Heisenberg spin chains, intrinsic spinon-spinon coupling alone is not resistive for magnetic heat transport according to theoretical calculations [6, 7]. The expected divergence of the intrinsic 1D magnetic thermal conductivity ( $\kappa_m$ ) makes the 1D spin chain an intriguing model system to study the celebrated Fermi-Pasta-Ulam-Tsingou (FPUT) problem [8, 9] of nonlinear dynamics in 1D systems. It is thus encouraging that a high magnetic contribution to the thermal conductivity ( $\kappa$ ) has been measured in several 1D magnetic systems with strong exchange interactions [10, 11]. In these experiments, the finite  $\kappa_m$  is attributed to extrinsic spinon coupling with defects [12-15], grain boundaries [16], and other quasiparticles such as phonons [13, 17, 18] and charge carriers [19, 20]. Thus, thermal transport measurements provide a useful probe of fundamental spinon transport length scales and coupling mechanisms, which cannot be readily obtained from other established methods. Meanwhile, for the spinon-induced SSE that was observed recently in the spin chain  $\text{Sr}_2\text{CuO}_3/\text{Pt}$  hybrid structure [3, 4], the SSE signal was found to be decreased by impurities in  $\text{Sr}_2\text{CuO}_3$  due to the suppression of spin transport, and an unusual temperature dependence of the SSE was further attributed to spinon-phonon coupling [4]. The importance of extrinsic spinon coupling mechanisms in both magnetic heat transport and SSE has motivated theoretical investigations [21-23]. In contrast to empirical expressions for spin-phonon coupling [24], recent theoretical studies have suggested a relatively weak upper bound for spinon-phonon coupling in the  $S=1/2$  Heisenberg spin chains [22, 25]. However, experimental determinations of spinon-phonon coupling have been hindered by the lack of knowledge of the defect concentration, which was often taken as an adjustable fitting parameter [26], and the

difficulty to separate  $\kappa_m$  and the lattice thermal conductivity ( $\kappa_l$ ), the latter of which had to be assumed to be isotropic in several previous studies of  $\kappa_m$  in the anisotropic systems [12, 24, 27].

In this Letter, we present experiments that are designed to quantify extrinsic spinon coupling with defects and phonons in the  $S=1/2$  Heisenberg spin chain compound  $\text{Ca}_2\text{CuO}_3$ , the thermal transport properties of which had not been studied previously. The defect concentration due to chain breaking is obtained from the measured specific heat ( $C_p$ ), an approach that has not been used in previous studies of spinon thermal transport. **Based on recent progress in accurate first-principles calculations of the thermal properties [28]**, first-principles phonon dispersions and  $\kappa_l$  calculations are employed here to allow for the determination of the temperature-dependent spinon mean free paths (MFPs) due to defect scattering and phonon scattering via a kinetic model of 1D spinon thermal transport. The obtained temperature dependence of the MFP provides experimental support of the recent theory [25] of weak spinon-optical phonon coupling, which has important implications for both spinon heat transport and spinon-driven SSE.

Single crystals of  $\text{Ca}_2\text{CuO}_3$  have been grown by the traveling-solvent floating zone (TSFZ) method [29]. The crystal structure of  $\text{Ca}_2\text{CuO}_3$  and an image of one of the crystals are shown in Figs. 1 (a) and (b), respectively. The material contains  $180^\circ$  Cu-O-Cu chains along  $b$  axis with a strong antiferromagnetic coupling energy  $J/k_B$  of  $\sim 2000$  K [43], **where  $k_B$  is the Boltzmann constant**. Figures 1(c) and (d) show a high-resolution transmission electron microscopy (TEM) micrograph and electron diffraction pattern of the crystal, respectively. The lattice spacing is found to be about 0.61 nm, in good agreement with the  $d$  value of the (200) plane in  $\text{Ca}_2\text{CuO}_3$ .

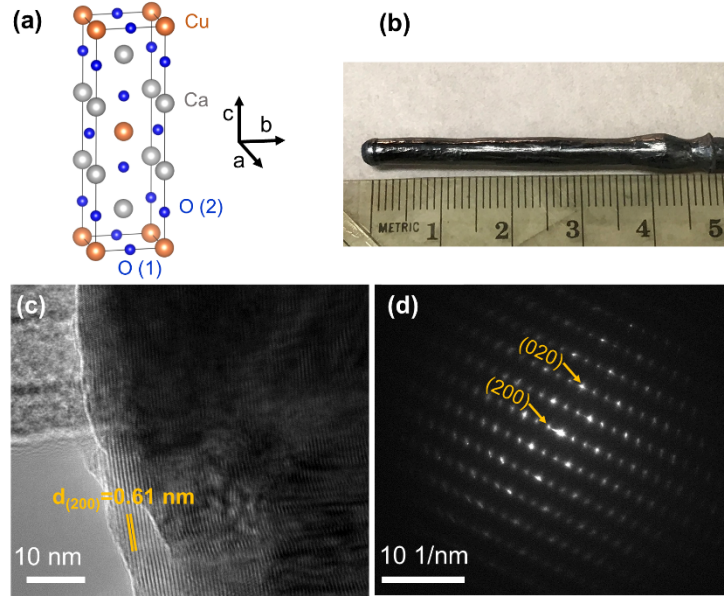


**Fig. 1.** (a) Crystal structure of  $\text{Ca}_2\text{CuO}_3$ . (b) A photo of a  $\text{Ca}_2\text{CuO}_3$  crystal grown by TSFZ method. (c) TEM image of the  $\text{Ca}_2\text{CuO}_3$  crystal. (d) The corresponding selected area electron diffraction pattern of  $\text{Ca}_2\text{CuO}_3$  in (c) obtained along the  $[001]$  zone axis.

Figure 2(a) shows the Raman spectrum of  $\text{Ca}_2\text{CuO}_3$  excited by 488 nm light at room temperature. The observed peak positions agree well with previous Raman studies [44-46]. The higher energy peaks with frequencies larger than  $685 \text{ cm}^{-1}$  are due to multi-phonon scattering. The magnetic excitation in 1D antiferromagnetic Heisenberg chains is a continuum with a lower bound described by a des Cloizeaux-Pearson dispersion,  $E(k) = \frac{1}{2} \pi J |\sin(k)|$ , and a higher bound given by the triplet excitation dispersion,  $E(k) = \pi J \left| \sin\left(\frac{1}{2}k\right) \right|$ , where  $E$  and  $k$  are the energy and wave vector of spinons, respectively [44]. The spinon continuum extends over a range from zero to over  $6000 \text{ cm}^{-1}$ , as indicated by the hump-like background in the Raman spectra. A broad peak is also observed around  $2200 \text{ cm}^{-1}$ , which is similar to the spinon-spinon pair states as reported in  $\text{Sr}_2\text{CuO}_3$  [47]. The interaction between the continuum of spinons and discrete optical phonon states leads to Fano asymmetric line shapes in some high-energy two-phonon peaks, such as the one at  $1401 \text{ cm}^{-1}$ .

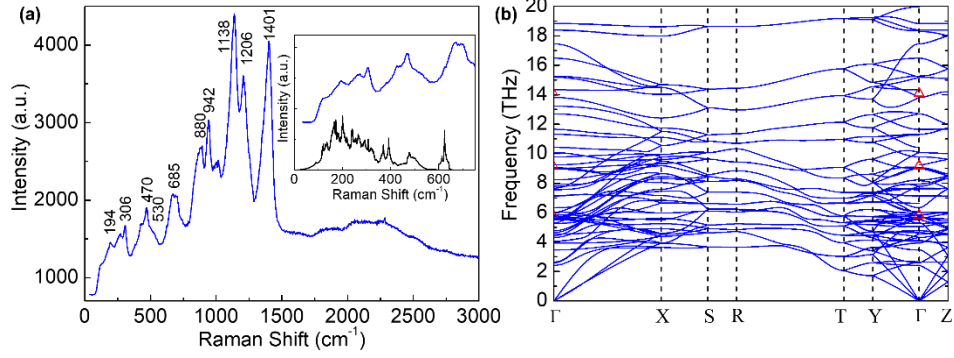


**Fig. 2.** (a) The measured Raman spectrum of  $\text{Ca}_2\text{CuO}_3$  at room temperature. The inset shows the Raman spectrum (blue curve) in comparison with phonon density of states from *ab initio* calculations (black curve). (b) Calculated phonon dispersion of  $\text{Ca}_2\text{CuO}_3$ . The red triangles are the measured Raman frequencies at 194, 306 and 470  $\text{cm}^{-1}$ .

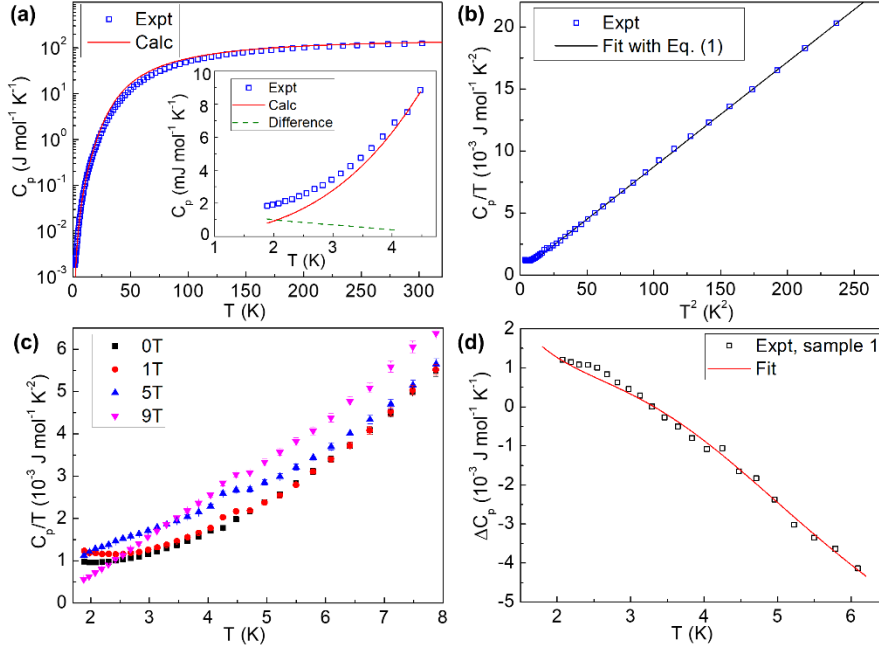
To calculate the phonon dispersion of  $\text{Ca}_2\text{CuO}_3$ , we combine a set of harmonic force constants obtained by a finite-difference method with a non-analytic correction to the dynamical matrix [29, 48]. Figure 2(b) shows the resulting phonon bands, plotted along a path passing through a representative set of high-symmetry points in the Brillouin zone. A particularly interesting feature of the dispersion is the clean folding of the bands at the boundaries along the  $b$  axis ( $\Gamma$ -Y), without clear evidence of symmetry breaking, e.g. the formation of minigaps. In other words, the effect of the lowered symmetry due to the magnetic order on the phonon bands is not remarkable. This fact provides support for our use of this dispersion even above the Néel temperature later on. In addition, the calculated phonon density of states (DOS) is qualitatively consistent with the measured Raman spectra, as shown in the inset in Fig. 2(a).

Figure 3(a) shows the temperature dependence of  $C_p$  for  $\text{Ca}_2\text{CuO}_3$ . The lattice contribution ( $C_l$ ) to the  $C_p$  is obtained from the calculated phonon dispersion [29]. The calculated value agrees well with the experimental data **except at the very low temperature range**, as shown in Fig. 3(a). Below  $\sim 4$  K, the difference between the calculated and experimental data is due to the magnetic contribution.

At low temperatures, the  $C_p$  in the electrically insulating  $\text{Ca}_2\text{CuO}_3$  consists of  $C_l$  and a contribution from magnetic excitations ( $C_m$ ) as [27]

$$C_p(T) = C_l + C_m = \frac{12xN_A\pi^4k_B}{5} \left(\frac{T}{\theta_D}\right)^3 + \frac{2yN_Ak_B^2}{3} \left(\frac{T}{J}\right), \quad (1)$$

where  $N_A$  is Avogadro's constant,  $T$  is temperature,  $\theta_D$  is the Debye temperature,  $x$  is the number of atoms per formula unit, and  $y$  is the number of magnetic atoms per formula unit. The fitting of low- $T$   $C_p$  in the 6 K to 15 K range according to Eq. (1) is shown in Fig. 3(b). The estimated  $\theta_D$  of  $\text{Ca}_2\text{CuO}_3$  is about 521 K, which is larger than the value of 448 K for  $\text{Sr}_2\text{CuO}_3$  [49].



**Fig. 3.** (a) Temperature dependence of  $C_p$  for  $\text{Ca}_2\text{CuO}_3$  in comparison with the calculated  $C_l$  based on phonon dispersion (red line). The inset is the difference between the calculated phonon contribution and measured  $C_p$  at low temperatures. (b) A plot of  $C_p(T)/T$  vs  $T^2$ . The black line is the fitting curve according to Eq. (1). (c)  $C_p(T)/T$  of a  $\text{Ca}_2\text{CuO}_3$  crystal plotted as a function of temperature under various applied magnetic fields. (d) Specific heat difference  $\Delta C_p$  obtained by subtracting  $C_p$  of  $\text{Ca}_2\text{CuO}_3$  under fields of 5 T and 9 T. The red line is the fitting curve according to Eq. (2).

Figure 3(c) shows the temperature dependence of  $C_p$  under various applied magnetic fields. There is an obvious upturn below 2.5 K observed in this sample and another sample [29] in the absence

of the magnetic field. Such an anomaly could be caused by a Schottky contribution [49, 50] due to the uncompensated spin-1/2 at the ends of fragmented chain segments. In the presence of defects, such as non-stoichiometry on copper or oxygen sites or impurity phases, 1D spin chains can break into even-length and odd-length segments, which have an even and an odd number of Cu sites, respectively. If the defect concentration is  $n_d$ , the average defect concentration due to the odd-length or even-length segments is about  $0.5n_d$ . The odd-length chains can introduce an additional contribution to  $C_p$  at low temperatures given by [51]

$$C_{Sch} = (n_d/2)R(\Delta_g/T)^2 \exp(\Delta_g/T)/[1 + \exp(\Delta_g/T)]^2 \quad (2)$$

where  $\Delta_g$  is the energy level splitting, and  $R$  is the ideal gas constant. To determine  $n_d$ , we analyzed the difference between the specific heat ( $\Delta C_p = C_{p,H1} - C_{p,H2}$ ) measured at two different magnetic fields. Based on this method, the effect of lattice and spinon contributions can be minimized [50]. The  $\Delta C_p$  data are fitted using the Schottky expression taking  $n_d$  and  $\Delta_g$  under different magnetic fields as the fitting parameters, as shown in Fig. 3 (d). The obtained fitting parameters are  $n_d = 0.0039$  per Cu ( $0.001 \text{ \AA}^{-1}$ ),  $\Delta_g = 1.2$  K at 5 T and  $\Delta_g = 25$  K at 9 T for sample 1. The sensitivity analysis and the  $C_p$  results for sample 2 can be found in Supplementary Material [29].

The  $\kappa$  of the  $\text{Ca}_2\text{CuO}_3$  crystals have been measured along all three crystallographic axes by a steady-state method [29], as shown in Fig. 4(a). The  $\kappa$  perpendicular to the spin chains ( $\kappa_a$  and  $\kappa_c$ ) show similar absolute values and temperature dependence. However, the  $\kappa$  along the chains ( $\kappa_b$ ) is much larger, especially from 70 K to 300 K. Because  $\text{Ca}_2\text{CuO}_3$  is an insulator, the higher  $\kappa$  along the chains has to be attributed to either a larger  $\kappa_l$  along  $b$ , or magnetic excitations, as observed in other spin chain compounds  $\text{SrCuO}_2$  and  $\text{Sr}_2\text{CuO}_3$  [24, 26, 27]. In addition, the peak  $\kappa$  of a polycrystalline sample is suppressed due to grain boundary scattering of phonons and



spinons, in agreement with recent thermal transport measurements of polycrystalline  $\text{Sr}_{14}\text{Cu}_{24}\text{O}_{41}$  [16].

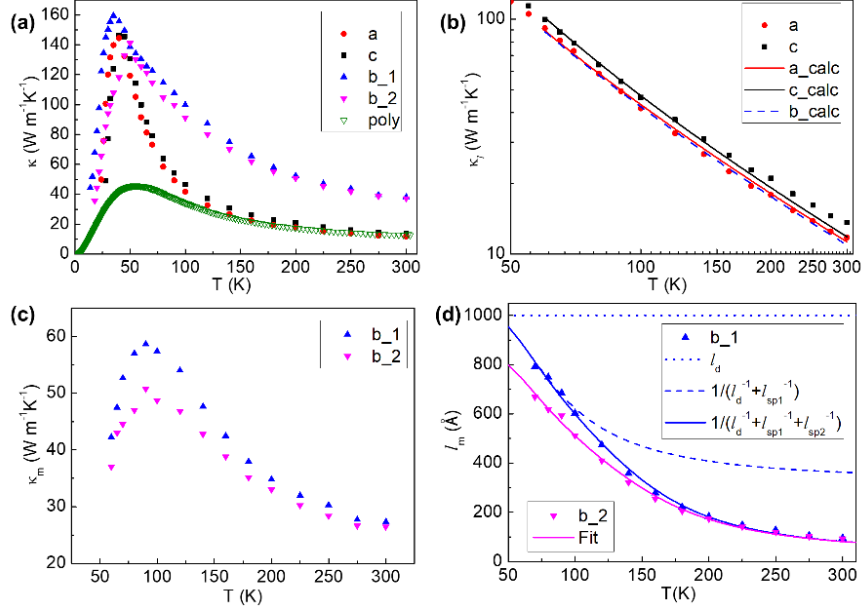


**Fig. 4.** (a) Thermal conductivity of  $\text{Ca}_2\text{CuO}_3$  crystals measured along the three principal crystallographic axes, in comparison with the  $\kappa$  of a  $\text{Ca}_2\text{CuO}_3$  polycrystalline sample. (b) Fit to the  $\kappa$  along the  $a$  and  $c$  axes. The blue dashed line is the calculated  $\kappa_i$  along the  $b$  axis. The details can be found in Supplementary Material [29]. (c) The extracted  $\kappa_m$  of  $\text{Ca}_2\text{CuO}_3$  along the  $b$  axis. (d) Calculated spinon MFP of  $\text{Ca}_2\text{CuO}_3$  along the  $b$  axis. The solid and dashed lines are the fits according to Eqs. (4-6).

We use the *ab initio* phonon results to calculate the  $\kappa_i$  and separate the spinon contribution. To focus on the intrinsic phonon transport behavior of the compound and remove the influence of the boundaries of our specific samples, we focus on the temperature range above  $\sim 70$  K. In the Boltzmann transport framework, we first fit the  $\kappa$  along  $a$  and  $c$  axes [29], along which any magnetic contribution should be negligible. The good agreement between the fitting model and the measurement data is shown in Fig. 4(b). The  $\kappa_i$  along  $b$  axis was calculated using the obtained fitting parameters and phonon dispersion. Despite an anisotropic crystal structure, the obtained  $\kappa_i$  are relatively isotropic along the three axes. Figure 4(c) shows the obtained  $\kappa_m$  for two samples

by subtracting  $\kappa_l$  from  $\kappa$ . The  $\kappa_m$  is about  $27 \text{ Wm}^{-1}\text{K}^{-1}$  at 300 K, and increases with decreasing temperature until the appearance of a peak  $\kappa_m$  value of  $50\text{-}60 \text{ Wm}^{-1}\text{K}^{-1}$  at about 90 K.

We now determine the spinon MFP ( $l_m$ ) by analyzing the  $\kappa_m$ . The  $\kappa_m$  in a 1D system can be expressed as  $\kappa_m = \int c_{m,k} v_{m,k} l_{m,k} dk$  and  $v_m$  is the spinon group velocity,  $v_m = \pi Jb/2\hbar$ , where  $b$  is the distance between the spins along the chains, and  $\hbar$  is the reduced Plank constant. For  $k_B T \ll J$ , the heat-carrying spinons exist in significant number only in the vicinity of the band minima [10, 52]. Therefore, it is adequate to assume that  $l_m = l_{m,k}$  in order to obtain a relation between the MFP of spinons and the  $\kappa_m$  of a 1D system as [26, 53]

$$l_m = \frac{3\hbar}{\pi N_s k_B^2 T} \kappa_m \quad (3)$$

where  $N_s = 2/ac$  is the number of spin chains per unit area. In addition, the two-spinon continuum is not considered here since most of the excited spinons exist in the vicinity of the band minima for temperatures below 300 K [10, 52]. As shown in Fig. 4(d),  $l_m$  of  $\text{Ca}_2\text{CuO}_3$  is about  $800 \text{ \AA}$  at 70 K for sample 1, corresponding to about 210 lattice spacings of  $b$ . With increasing temperature,  $l_m$  is reduced and approaches a constant value of  $\sim 100 \text{ \AA}$  at 300 K for both samples.

In the temperature range for this study, heat transport by spinons is mainly limited by the spinon-defect scattering and spinon-optical phonon scattering processes [25]. The  $J$  is a function of the Cu-Cu separation that can be perturbed by thermal lattice vibrations. This perturbation provides the mechanism for coupling phonons to the spinons [21]. A recent theory has expressed the MFP due to the spinon-phonon scattering ( $l_{sp}$ ) as [25]

$$l_{sp}^{-1} = g_{sp}^2 \frac{2J}{k_B T a} \frac{1}{\sinh(2\pi\hbar\omega_0/k_B T)} \quad (4)$$

where  $g_{sp}$  is the spinon-phonon coupling constant, and  $\omega_0$  is the frequency of the phonon mode.

In addition, spinons can also be affected by impurities, which perturb the superexchange coupling locally. In effect, the defects can act like breaches in the spin chain. The corresponding MFP is an average length of a defect-free chain, which is given by [25]

$$l_d^{-1} = n_d. \quad (5)$$

To model the MFP of spinons, we have combined spinon-phonon and spinon-defect scattering according to Matthiessen's rule as

$$l^{-1} = l_{sp}^{-1} + l_d^{-1}. \quad (6)$$

In addition, we have assumed that the spinons are scattered by two optical phonon modes:  $\omega_{0,1} = 6.25$  THz and  $\omega_{0,2} = 19.17$  THz [25]. In our analysis, these two frequency values are the representative average values determined according to the effect of phonon modes on the degrees of freedom of Cu atoms along  $b$  axis [29]. The first mode represents a broad distribution of phonon energy ( $E$ ) centered at  $E/k_B = 300$  K. The latter corresponds to the stretching mode at  $E/k_B = 920$  K. The solid lines in Fig. 4(d) are the fits of the  $l_m$  for  $\text{Ca}_2\text{CuO}_3$ . With  $J/k_B = 2200$  K, the obtained optimum fitting parameters are  $n_d = 0.00099 \text{ \AA}^{-1}$ ,  $g_{sp,1} = 0.023$ , and  $g_{sp,2} = 0.16$  for sample 1, and  $n_d = 0.0012 \text{ \AA}^{-1}$ ,  $g_{sp,1} = 0.025$ , and  $g_{sp,2} = 0.16$  for sample 2. Sensitivity analysis [29] shows that these are unique fits to the data. The larger  $n_d$  for sample 2 can explain its lower  $\kappa_m$  below  $\sim 150$  K. The obtained  $n_d$  agrees well with the value of  $0.001 \text{ \AA}^{-1}$  derived from the  $C_p$  data. In comparison, prior experimental and theoretical studies [21, 24, 27] on analyzing the spinon-phonon scattering MFP assumed a  $g_{sp} \geq 1$ . Based on the perturbative treatment of spinon-phonon scattering, however, recent theoretical studies [22, 25] indicate that the upper limit on the spin-phonon coupling in 1D cuprates is  $\sim 0.2$ . Our experimental findings are consistent with the recent theoretical work, confirming the relative weak coupling between spinons and phonons in 1D Heisenberg  $S=1/2$  spin chain compounds. Moreover, based on the calculated MFP due to different scattering processes, defect scattering is dominant below  $\sim 50$  K, which can explain the suppressed SSE signal in low-purity  $\text{Sr}_2\text{CuO}_3$  below  $\sim 50$  K [4]. In comparison, the spinon

scattering is mainly limited by phonon scattering above  $\sim 50$  K. Despite its small coupling constant, the  $\omega_{0,1}$  mode is more effective in scattering spinons than the  $\omega_{0,2}$  mode below 100 K.

The  $\omega_{0,2}$  mode starts to play a more important role at higher temperatures.

These experiments and analysis yield quantitative insight into spinon coupling with defects and phonons in single crystals of  $\text{Ca}_2\text{CuO}_3$ , which is considered to be a model system for strongly anisotropic spin-1/2 Heisenberg antiferromagnets. Spin chain breaking due to the presence of defects results in the observed Schottky anomaly in  $C_p$  at low temperature. The magnetic field-dependent  $C_p$  indicates a defect concentration of  $0.001 \text{ \AA}^{-1}$ . Meanwhile, determination of  $\kappa_l$  from the phonon dispersion has enabled its separation from the measured  $\kappa$  to obtain the large magnetic contribution  $\kappa_m$ . Based on the knowledge of the defect concentration and  $\kappa_m$ , the spinon MFP is obtained from a kinetic model of 1D spinon transport, which decreases from  $\sim 800 \text{ \AA}$  at 70 K to  $\sim 100 \text{ \AA}$  at 300 K. The MFP results suggest that defect scattering is the leading mechanism below 50 K while optical phonon scattering is dominant at high temperature, and provide experimental support of the recent theory of weak spinon-phonon coupling. Moreover, the methods presented in this work can be applicable to probe fundamental length scales in other low-D magnetic systems.

## Acknowledgements

This work was supported by US Army Research Office (ARO) MURI award W911NF-14-1-0016. The phonon dynamics calculation was performed using HPC resources from GENCI-TGCC (project A0030910242). The SPS processing at The University of Texas at Austin was conducted with the instrument acquired with the support of NSF award number DMR-1229131. The crystal growth and the specific heat measurement were made possible by using the facility supported by

NSF through the Center for Dynamics and Control of Materials: an NSF MRSEC under Cooperative Agreement No. DMR-1720595.

## References

- [1] M. Uehara, T. Nagata, J. Akimitsu, H. Takahashi, N. Mōri, and K. Kinoshita, *J. Phys. Soc. Jpn* **65**, 2764 (1996).
- [2] J. Schlappa *et al.*, *Nature* **485**, 82 (2012).
- [3] D. Hirobe, M. Sato, T. Kawamata, Y. Shiomi, K.-i. Uchida, R. Iguchi, Y. Koike, S. Maekawa, and E. Saitoh, *Nat. Phys.* **13**, 30 (2017).
- [4] D. Hirobe, T. Kawamata, K. Oyanagi, Y. Koike, and E. Saitoh, *J. Appl. Phys.* **123**, 123903 (2018).
- [5] S. Sahling *et al.*, *Nat. Phys.* **11**, 255 (2015).
- [6] X. Zotos, F. Naef, and P. Prelovsek, *Phys. Rev. B* **55**, 11029 (1997).
- [7] F. Heidrich-Meisner, A. Honecker, D. C. Cabra, and W. Brenig, *Phys. Rev. B* **68**, 134436 (2003).
- [8] E. Fermi, J. Pasta, and S. Ulam, Los Alamos National Laboratory, Document LA-1940 (1955).
- [9] J. L. Tuck and M. T. Menzel, *Adv. Math.* **9**, 399 (1972).
- [10] C. Hess, *Eur. Phys. J. Spec. Top.* **151**, 73 (2007).
- [11] A. V. Sologubenko, T. Lorenz, H. R. Ott, and A. Freimuth, *J. Low Temp. Phys.* **147**, 387 (2007).
- [12] A. Mohan, N. S. Beesetty, N. Hlubek, R. Saint-Martin, A. Revcolevschi, B. Büchner, and C. Hess, *Phys. Rev. B* **89**, 104302 (2014).
- [13] N. Hlubek, P. Ribeiro, R. Saint-Martin, A. Revcolevschi, G. Roth, G. Behr, B. Büchner, and C. Hess, *Phys. Rev. B* **81**, 020405 (2010).
- [14] C. Hess, B. Büchner, U. Ammerahl, L. Colonescu, F. Heidrich-Meisner, W. Brenig, and A. Revcolevschi, *Phys. Rev. Lett.* **90**, 197002 (2003).
- [15] C. Hess, P. Ribeiro, B. Büchner, H. ElHaes, G. Roth, U. Ammerahl, and A. Revcolevschi, *Phys. Rev. B* **73**, 104407 (2006).
- [16] X. Chen, K. Jarvis, S. Sullivan, Y. Li, J. Zhou, and L. Shi, *Phys. Rev. B* **95**, 144310 (2017).
- [17] C. Hess, C. Baumann, and B. Büchner, *J. Magn. Magn. Mater.* **290**, 322 (2005).
- [18] M. Montagnese *et al.*, *Phys. Rev. Lett.* **110**, 147206 (2013).
- [19] C. Hess, H. ElHaes, B. Büchner, U. Ammerahl, M. Hücker, and A. Revcolevschi, *Phys. Rev. Lett.* **93**, 027005 (2004).
- [20] A. V. Sologubenko, K. Gianno, H. R. Ott, U. Ammerahl, and A. Revcolevschi, *Phys. Rev. Lett.* **84**, 2714 (2000).
- [21] A. L. Chernyshev and A. V. Rozhkov, *Phys. Rev. B* **72**, 104423 (2005).
- [22] A. L. Chernyshev and W. Brenig, *Phys. Rev. B* **92**, 054409 (2015).
- [23] K. Louis, P. Prelovšek, and X. Zotos, *Phys. Rev. B* **74**, 235118 (2006).
- [24] N. Hlubek, X. Zotos, S. Singh, R. Saint-Martin, A. Revcolevschi, B. Büchner, and C. Hess, *J. Stat. Mech. Theory Exp.* **2012**, P03006 (2012).
- [25] A. L. Chernyshev and A. V. Rozhkov, *Phys. Rev. Lett.* **116**, 017204 (2016).
- [26] A. V. Sologubenko, K. Gianno, H. R. Ott, A. Vietkine, and A. Revcolevschi, *Phys. Rev. B* **64**, 054412 (2001).
- [27] A. V. Sologubenko, E. Felder, K. Gianno, H. R. Ott, A. Vietkine, and A. Revcolevschi, *Phys. Rev. B* **62**, R6108 (2000).

- [28] J. Carrete, B. Vermeersch, A. Katre, A. van Roekeghem, T. Wang, G. K. H. Madsen, and N. Mingo, *Comput. Phys. Commun.* **220**, 351 (2017).
- [29] See Supplemental Material for more details on synthesis methods, phase and microstructure characterization, specific heat and thermal conductivity measurements, first-principles calculations of phonon dispersion and lattice thermal conductivity, projected phonon density of states, fat-bands plot and sensitivity analysis, **which includes Refs. [30-42]**.
- [30] J. Wada, S. Wakimoto, S. Hosoya, K. Yamada, and Y. Endoh, *Physica C: Supercond.* **244**, 193 (1995).
- [31] H. Dang-Chinh, N. Duc-The, and H. Nam-Nhat, *J. Phys.: Condens. Matter* **19**, 106215 (2007).
- [32] N. C. Hyatt, L. Gray, I. Gameson, P. P. Edwards, and S. Hull, *Phys. Rev. B* **70**, 214101 (2004).
- [33] G. Simutis *et al.*, *Phys. Rev. B* **95**, 054409 (2017).
- [34] X. Chen, S. N. Girard, F. Meng, E. Lara-Curzio, S. Jin, J. B. Goodenough, J. S. Zhou, and L. Shi, *Adv. Energy Mater.* **4**, 1400452, 1400452 (2014).
- [35] W. Schnelle, R. Fischer, and E. Gmelin, *J. Phys. D: Appl. Phys.* **34**, 846 (2001).
- [36] G. Kresse and J. Hafner, *Phys. Rev. B* **47**, 558 (1993).
- [37] G. Kresse and J. Furthmüller, *Phys. Rev. B* **54**, 11169 (1996).
- [38] G. Kresse and J. Furthmüller, *Comp. Mater. Sci.* **6**, 15 (1996).
- [39] G. Kresse and D. Joubert, *Phys. Rev. B* **59**, 1758 (1999).
- [40] J. P. Perdew, K. Burke, and M. Ernzerhof, *Phys. Rev. Lett.* **77**, 3865 (1996).
- [41] W. Tang, E. Sanville, and G. Henkelman, *J. Phys.: Condens. Matter* **21**, 084204 (2009).
- [42] A. Togo and I. Tanaka, *Scripta Mater.* **108**, 1 (2015).
- [43] K. Foyevtsova, J. T. Krogel, J. Kim, P. R. C. Kent, E. Dagotto, and F. A. Reboredo, *Phys. Rev. X* **4**, 031003 (2014).
- [44] S. Sugai, J. Wada, K. Yamada, S. Hosoya, and Y. Endoh, *Physica B: Condens. Matter* **219-220**, 505 (1996).
- [45] M. Yoshida, S. Tajima, N. Koshizuka, S. Tanaka, S. Uchida, and S. Ishibashi, *Phys. Rev. B* **44**, 11997 (1991).
- [46] N. N. Hoang, D. C. Huynh, T. T. Nguyen, D. T. Nguyen, D. T. Ngo, M. Finnie, and C. Nguyen, *Appl. Phys. A* **92**, 715 (2008).
- [47] O. V. Misochko, S. Tajima, C. Urano, H. Eisaki, and S. Uchida, *Phys. Rev. B* **53**, R14733 (1996).
- [48] Y. Wang, J. J. Wang, W. Y. Wang, Z. G. Mei, S. L. Shang, L. Q. Chen, and Z. K. Liu, *J. Phys.: Condens. Matter* **22**, 202201 (2010).
- [49] K. Karmakar, R. Bag, M. Skoulatos, C. Rüegg, and S. Singh, *Phys. Rev. B* **95**, 235154 (2017).
- [50] A. P. Ramirez, S. W. Cheong, and M. L. Kaplan, *Phys. Rev. Lett.* **72**, 3108 (1994).
- [51] J. G. Cheng, J. S. Zhou, J. B. Goodenough, Y. T. Su, Y. Sui, and Y. Ren, *Phys. Rev. B* **84**, 104415 (2011).
- [52] N. Hlubek, *Magnetic heat transport in one-dimensional quantum antiferromagnets*, Ph.D. thesis, Technische Universität Dresden (2010).
- [53] C. Hess, H. ElHaes, A. Waske, B. Büchner, C. Sekar, G. Krabbes, F. Heidrich-Meisner, and W. Brenig, *Phys. Rev. Lett.* **98**, 027201 (2007).